

Hardware-efficient entangled measurements for variational quantum algorithms

Francisco Escudero^{1,2}, David Fernández-Fernández^{1,3}, Gabriel Jaumà¹, Guillermo F. Peñas¹, and Luciano Pereira¹

¹Instituto de Física Fundamental, IFF-CSIC, Calle Serrano 113b, 28006 Madrid, Spain

²CWI & QuSoft, Science Park 123, 1098 XG Amsterdam, The Netherlands

³Instituto de Ciencia de Materiales de Madrid, ICMM-CSIC, E-28049 Madrid, Spain

Variational algorithms have received significant attention in recent years due to their potential to solve practical problems in noisy intermediate-scale quantum (NISQ) devices. A fundamental step of these algorithms is the evaluation of the expected value of Hamiltonians, and hence, efficient schemes to perform this task are required. The standard approach employs local measurements of Pauli operators and requires a large number of circuits. An alternative is to make use of entangled measurements, which significantly reduces the number of circuits but involves entangling gates between non-physically connected qubits, introducing intermediate entangling operations that increase the depth of the circuits. As a solution to this problem we propose hardware-efficient entangled measurements (HEEM), that is, measurements that only permit entanglement between physically connected qubits. We show that this strategy enhances the evaluation of molecular Hamiltonians in NISQ devices, reducing the number of circuits required without increasing their depth. We provide quantitative metrics of how this approach offers better results than only local measurements and arbitrarily entangled ones. We estimate with classical simulators and quantum hardware the ground state energy of the H₂O molecule by the variational quantum eigensolver using HEEM.

1 Introduction.

We are currently in the era of noisy intermediate-scale quantum (NISQ) computers. The main limitations of these devices are short coherence times and noisy entangling gates, thus, NISQ circuits must inevitably have a low depth [1]. Given that, a lot of effort has been devoted to the design and implementation of quantum algorithms that only use low-depth circuits [2–5]. Among such algorithms, one of the

families that has gained attention are the variational quantum algorithms (VQAs) [6–8]: hybrid quantum-classical methods where a classical computer guides a quantum computer to produce variational quantum states and to measure their expected value, with the goal of minimizing an objective function encoded in a quantum Hamiltonian. The most famous VQAs are the variational quantum eigensolver (VQE) [9] and the quantum approximate optimization algorithm (QAOA) [10]. Multiple VQAs have been applied in a wide range of areas such as chemistry [11–14], finance [15, 16], traffic prediction [17], machine learning [18–21], entanglement detection [22–24] and differential equations [25–27].

Despite the great advances made in recent years, implementing VQA is still challenging. One of the main drawbacks is the number of measurements required to evaluate the objective function. Such evaluation can be done by decomposing the Hamiltonian on a basis of tensor products of Pauli operators, also called Pauli strings, and then measuring each of these terms independently. Using this approach, the number of measurements needed to evaluate the objective function is equal to the Pauli terms of the Hamiltonian, which scales as N^4 for typical instances such as second-quantized chemical Hamiltonians on N qubits [28]. The preparation and measurement of each circuit require a non-negligible amount of time and resources, thus, decreasing the number of circuits is essential to speed up VQAs and to reach realistic applications of quantum computing.

Several methods have been proposed to reduce the total number of measurements required for each energy evaluation, such as classical shadows [29, 30], quantum tomography [31–33], or machine learning [34–36], among others [37–40]. Other proposals are grouping methods, which exploit the commutative relation between the Pauli strings to make groups that can be measured simultaneously, reducing the number of required experiments. The most widely known approach is the grouping with tensor product basis (TPB) [12–14, 41, 42], which use qubit-wise commutativity and require no entanglement. Another alternative is to use entangled measurements, which fur-

ther reduce the number of measurements compared to TPB [28, 43–45]. However, this last approach assumes unlimited entanglement resources, and hence is not suitable for NISQ devices. There is a midpoint between the two extreme alternatives of assuming limitless entanglement or none at all: using measurements whose entanglement requirements are within the limits of NISQ devices. There are several works in this line [46–49], nevertheless, none of these techniques takes into account the connectivity of the particular quantum processor where the algorithm is run.

In this article, we address the problem of grouping Pauli strings with entangled measurements (EMs), but only between physically connected qubits, that is, hardware-efficient entangled measurements (HEEMs). Given a set of Pauli strings and a processor connectivity, there is a vast number of possible HEEMs, some of which will be more effective than others. Finding the optimal HEEM requires, among other things, finding the optimal mapping between the theoretical qubits of the algorithm and the physical qubits of the device. We have named this the *processor embedding* problem. We propose heuristic algorithms to solve the processor embedding problem and to perform the grouping with HEEMs. We run VQE with HEEM to estimate the ground state energy of the H_2O molecule using both classical simulators and quantum hardware. The method reduces the number of measurements, thanks to the entangled measurements, and avoids long-range qubit interactions that would involve noisy, deep circuits, thanks to the hardware-efficient approach.

2 Hardware-efficient grouping

A general N -qubit Hamiltonian can be expanded in terms of Pauli strings as

$$H = \sum_{\alpha} h_{\alpha} P_{\alpha}, \quad (1)$$

where P_{α} are the tensor products of the identity and Pauli operators (I, X, Y, Z), and $h_{\alpha} \in \mathbb{R}$ are the coefficients of each Pauli string. The standard routine to compute the expected value of H consists of measuring each Pauli string P_i with a Tensor Product Basis (TPB), which are the tensor products of the bases of eigenstates of the Pauli operators $\{\mathcal{X}, \mathcal{Y}, \mathcal{Z}\}$, with $\mathcal{X} = \{|0\rangle \pm |1\rangle\}$, $\mathcal{Y} = \{|0\rangle \pm i|1\rangle\}$, and $\mathcal{Z} = \{|0\rangle, |1\rangle\}$.

Multiple Pauli strings can be evaluated simultaneously with a single TPB. In this case, we say that they are *compatible* with that TPB. For instance, the 3-qubit Pauli strings XIZ and XYZ are compatible with the TPB $\mathcal{X} \otimes \mathcal{Y} \otimes \mathcal{Z}$. This property allows us to define a grouping method [41], which consists of searching for the smallest set of TPB that can be used to evaluate the expected value of H . Finding the best TPB grouping for a given Hamiltonian is equivalent

to finding the best coloring for its Pauli graph, which is NP-complete [42, 50].

One can go beyond the TPB grouping and measure the expected value of H with fewer groups thanks to entangled measurements (EM), that is, measuring after an entangling operation. In [46] the authors proposed a heuristic algorithm to construct groups using EM between pairs of qubits (Appendix B for further details). Grouping with EM proved to be more efficient than grouping with TPB, significantly reducing the number of measurements and the uncertainty on the evaluation of observables. One drawback of this approach is that it neglects the error of entangling gates in NISQ devices, and hence it might actually worsen the results in some scenarios. This is particularly pronounced when performing entangling operations between non-physically-connected qubits, since these require the usage of mediating qubit—and hence additional entangling gates—that increase the depth and thus the error of the circuits.

As a solution to this problem, we propose three heuristic algorithms to group Pauli strings with HEEM (see Appendix A of the supplementary material). These algorithms introduce two important improvements to the algorithm proposed by Hamamura *et al.* [46]. First, they check whether two Pauli strings are simultaneously measurable by an EM given the connectivity of a device (algorithm 2), isolating from all possible EM only those that are hardware-efficient. Second, since the groups obtained by our algorithms or by Hamamura's depends on the order followed by several loops, we introduce three algorithms to choose these orders. This is explained in the following section.

2.1 The processor embedding problem

There are multiple factors that determine the performance of the grouping algorithm 1, for instance, the order that its loops follow to run through the qubits, the assignable measurements, and the Pauli strings. These orders can be optimized considering what we have named the *processor embedding problem*: the problem of finding the optimal way to map the theoretical qubits of the Hamiltonian into the physical qubits of the device. In this section, we introduce a heuristic approach to solve this problem, which in turn allows us to optimize the order of the loops in the qubits and in the assignable measurements.

Given the Hamiltonian shown in Eq. (1), its *compatibility matrix* C is a $N \times N$ symmetric matrix whose non-diagonal entries C_{ij} are equal to the number of compatible entangled measurements (see Table 2 in the Supp. Material) that involve qubits i and j . The non-diagonal entries of C are not relevant for the *processor embedding problem*.

The number of compatible entangled measurements that involve qubits (i, j) is defined in the following

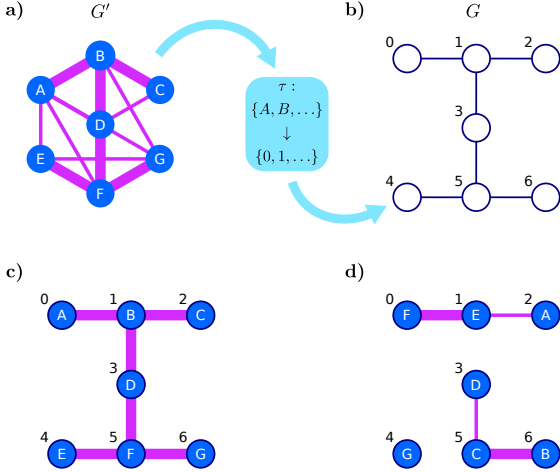


Figure 1: Schematic representation of the processor embedding problem. **a)** Compatibility graph of theoretical qubits, G' . Given a set of Pauli strings, the width of the edges $\{i, j\}$ of this graph represents the number of entangled measurements that can be established between qubits i and j , C_{ij} . **b)** Connectivity graph of the physical qubits of the `ibmq_jakarta` device, G . **c)** and **d)** are good and bad processor embedding maps τ , respectively.

way. The factors i and j of each Pauli string P_α can be regarded as a set of Pauli sub-strings of 2 qubits, $\{P_\alpha^{i,j}\}$, and the number of compatible entangled measurements that involve qubits (i, j) is the number of pairs of Pauli sub-strings $\{P_\alpha^{i,j}\}$ that are compatible through an entangled measurement. Thus, the compatibility matrix encapsulates how many entangled measurements can be established between two qubits. As an example, let's consider the following set of Pauli strings

$$P_\alpha \begin{cases} XXZ \\ YYZ \\ YZZ \end{cases} \Rightarrow P_\alpha^{0,1} \begin{cases} XX \\ YY \\ YZ \end{cases} \Rightarrow C_{01} = C_{10} = 2.$$

In this example $C_{10} = C_{01} = 2$ because XX and YY can be simultaneously measured with a Bell measurement and XX and YZ with an Ω^X measurement (see Supp. Material B.2). However, YY and YZ cannot be measured simultaneously, i.e., $[YY, YZ] \neq 0$.

With the compatibility matrix, we can tackle the processor embedding problem by trying to maximize the number of potential entangled measurements between neighboring qubits. We formulate this problem in terms of graphs, as shown in Fig. 1. Let $G' := (V', E', C)$ be the weighted graph defined by the vertices $V' := \{1, \dots, N\}$, where N is the number of theoretical qubits, the edges $E' := V' \times V'$ and the weights C_{ij} . In this way, G' represents the compatibility between the theoretical qubits (Fig. 1 a)). Let $G := (V, E)$ be the graph defined by the vertices $V := \{1, \dots, M\}$, with $M \geq N$ the number of physical qubits and the edges $E := \{(i, j) \in V \times V : \text{qubits } i \text{ and } j \text{ that are physically connected}\}$. In this way, G represents the topology of the chip (Fig. 1 b)).

The objective is to find the map $\tau : \{1, \dots, N\} \rightarrow \{1, \dots, M\}$ that maximizes

$$\omega(\tau) = \sum_{\{(i,j) \in V' \times V' : (\tau(i), \tau(j)) \in E\}} C_{ij}. \quad (2)$$

Note that $\omega(\tau)$ is the total number of compatibilities between theoretical qubits once they are mapped to physical qubits through τ . For the example shown in Fig. 1 a), where thin edges correspond to $C_{ij} = 1$ and wide ones to $C_{ij} = 2$, the optimal processor embedding map (Fig. 1 c)) results in $\omega(\tau) = 12$, while a bad mapping (Fig. 1 d)) gives a lower value $\omega(\tau) = 6$.

The problem of finding the best τ is what we will refer to by the *processor embedding* problem, which we know is NP-hard and hence there is no efficient algorithm for the general case. There are several ways of proving that the processor embedding problem is NP-hard. For instance, the max-clique problem, which is itself NP-hard [51], can be regarded as the simplification of the processor embedding problem such that all non-diagonal entries of C are positive and equal. Additionally, the k -densest subgraph problem is NP-complete and can also be seen as a particular instance of the processor embedding problem [52, 53]. Efficient algorithms could be found for the physically relevant instances of the processor embedding problem if one finds some kind of structure within them. For now, we propose two heuristic algorithms (see Appendix A.2) to construct a map τ . The first is the *order disconnected* map, algorithm 4. Here, each pair of theoretical qubits (i, j) with the highest entries C_{ij} is mapped to physically connected qubits. The second alternative is the *order connected* map, algorithm 5. This algorithm does the same as the previous, but it additionally ensures that the graph $\tau(G')$ is a connected sub-graph of G . The third alternative is the *naive* map. This is simply the trivial map $\tau(i) = i$ for $i \in \{1, \dots, N\}$, and it allows us to benchmark our *order connected* and *order disconnected* maps.

Once the map τ has been chosen one can propose an order for the loops of our grouping algorithm (Algorithm 1), in the qubits and in the measurements, using the τ -compatibility matrix C^τ , defined by

$$C_{ij}^\tau := \begin{cases} C_{ij} & \text{if } (\tau(i), \tau(j)) \in E \\ 0 & \text{if } (\tau(i), \tau(j)) \notin E. \end{cases}$$

Let CQ_i^τ be the N -vector whose i entry is given by

$$CQ_i^\tau := C\mathcal{X}_i + C\mathcal{Y}_i + C\mathcal{Z}_i + \sum_{j \neq i} C_{ij}^\tau, \quad (3)$$

where $C\mathcal{X}_i$, $C\mathcal{Y}_i$ and $C\mathcal{Z}_i$ are the numbers of compatibilities involving qubit i through the measurements \mathcal{X} , \mathcal{Y} and \mathcal{Z} , respectively. In this way, CQ_i^τ is the number of compatibilities involving the qubit i , given that τ has been chosen as the processor embedding map. Now, its natural to propose the following order

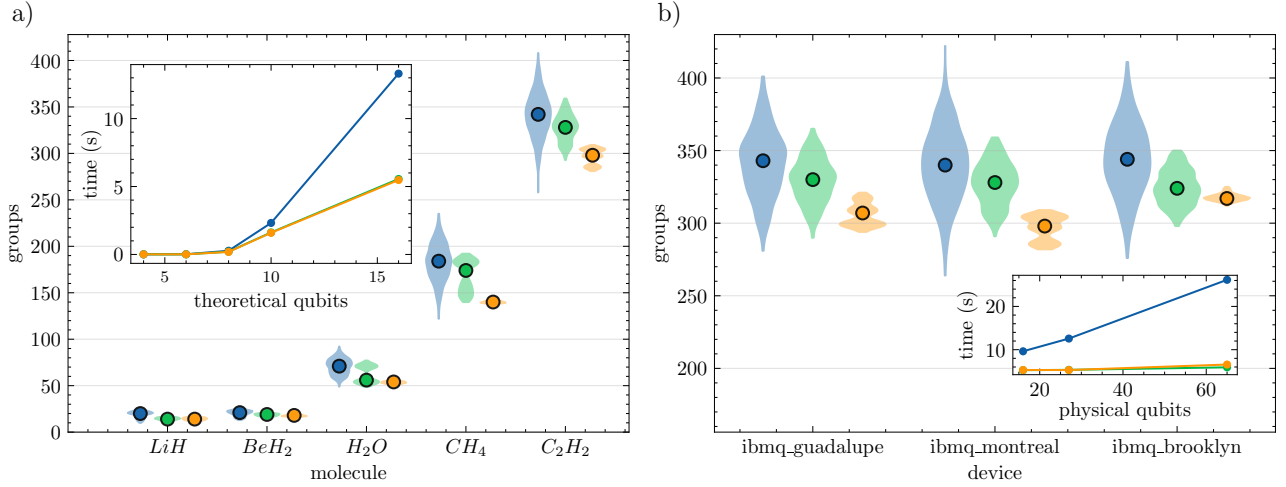


Figure 2: Results for grouping algorithms. The violins correspond to the distributions on the number of groups after running a Monte Carlo simulation over the order of the Pauli strings and the order of the theoretical qubits for different **a)** molecules, and **b)** devices. Blue violins correspond to the naive algorithm (Section 2.1), green violins correspond to the order disconnected algorithm (see Supp. Material, Algorithm 4), and orange violins to the order connected algorithm (see Supp. Material, 5). The colored dots represent the mean value in the number of groups in each case. The insets show the average execution time of the grouping algorithm. In **a)** the algorithms group according to HEEM with the connectivity of *ibmq_montreal*. In **b)** the number of groups corresponds to the C₂H₂ molecule.

for the qubits: *run through the qubits in descending order of CQ^τ*.

Let $CM^τ$ be the set of 9 tuples of the form

$$CM^τ := \{(\mathcal{X}, C\mathcal{X}), (\mathcal{Y}, C\mathcal{Y}), (\mathcal{Z}, C\mathcal{Z}), (Bell, C^T Bell), (\chi, C^τ \chi), (\tilde{\chi}, C^τ \tilde{\chi}), (\Omega^X, C^τ \Omega^X), (\Omega^Y, C^τ \Omega^Y), (\Omega^Z, C^τ \Omega^Z)\}, \quad (4)$$

where $C^T Bell$ is the number of compatibilities due to Bell measurement, since $τ$ has been chosen as the processor embedding map; $C^τ \chi$, $C^τ \tilde{\chi}$, $C^τ \Omega^X$, $C^τ \Omega^Y$ and $C^τ \Omega^Z$ are defined analogously. $C\mathcal{X}$, $C\mathcal{Y}$ and $C\mathcal{Z}$ are the numbers of compatibilities by the measurements \mathcal{X} , \mathcal{Y} , and \mathcal{Z} (these numbers do not depend on $τ$, because these measurements are separable). Now, it is natural to propose the following order for the measurements: *run through the measurements in descending order of CM^τ*. The order in which Algorithm 1 runs along the Pauli strings is independent of $τ$. It is chosen by the Pauli graph, visiting the Pauli strings in descending order with respect to their degree in this graph, similarly to what is done in largest-degree-first coloring (LDFC) algorithm [54].

Finally, we must emphasize that the processor embedding problem is not only relevant to choose the best orders for the loops of our grouping algorithm (Algorithm 1), but also affects the number of groups obtained. For example, suppose that we have $N = M = 3$, two Pauli strings XXZ and ZXX and $E = \{(0, 1), (1, 2)\}$. If we choose $τ : 0 \rightarrow 0, 1 \rightarrow 1, 2 \rightarrow 2$ we need to measure both strings separately, but choosing $\tilde{\tau} : 0 \rightarrow 1, 1 \rightarrow 0, 2 \rightarrow 2$ one measurement suffices. In addition, the processor embedding problem is crucial to reduce the error caused by gates in

NISQ computers, as a good choice of $τ$ would reduce the number of CNOTs used in the circuit, which is a relevant task in the physical layout problem [55]. Indeed, if we had to apply a theoretical CNOT in our algorithm between qubits i and j that are mapped to physical qubits whose distance in the chip is D , then in practice we would need to apply $\mathcal{O}(D)$ CNOTs between physically connected qubits, so reducing D using an appropriate $τ$ is essential. Also, in a real device the accuracy of CNOT gates between connected qubits will vary depending on the chosen qubits. If one takes into account these other tasks and not only the grouping, the weights of G' should vary: it should not only depend on the compatibility matrix, but also on those other features. This extension will be addressed in future works.

3 Results

We will begin by comparing the HEEM grouping algorithms that we have proposed: the naive, the order disconnected, and the order connected. The reasons that led us to develop the order connected and order disconnected methods were improving the naive method and reducing its dependence on the order followed in its loops. To verify the enhancements, we studied the statistical behavior of the three algorithms with a Monte Carlo simulation that randomly permutes the order of the theoretical qubits and of the Pauli strings used as input for the algorithms. Indeed, Figure 2 a) shows that the order connected and order disconnected algorithms are better on average than the naive algorithm, improving it, and that they have

	qubits	No grouping	TPB	EM	EM # CNOTs	HEEM	HEEM # CNOTs
H ₂	2	5	2	2	1	2	1
LiH	4	100	25	11	8	10	8
BeH ₂	6	95	24	15	74	13	18
H ₂ O	8	444	93	51	563	47	80
CH ₄	10	1191	246	113	2677	117	224
C ₂ H ₂	16	1884	457	189	8969	258	433

Table 1: Number of groups for some molecules using different grouping strategies. TPB groups have been obtained using the LDFC algorithm. EM groups are those proposed by [46]. HEEM groups have been obtained using algorithm 1 assuming that the physical qubits have the connectivity of the device *ibmq_montreal*.

less dispersion, reducing its dependence on the orders. It is true that the absolute minimum number of groups is obtained with the naive algorithm, however, this is not relevant in practice, since one would like to run the algorithm just once. It is also remarkable that on both average and dispersion, the order-connected algorithm is the one that performs best. These results seem to imply that the order-disconnected—and more so the order-connected—algorithms explore a region of the space of solutions that is narrower and better on average than the naive algorithm.

In terms of time execution, the order-connected and order-disconnected algorithms are much faster than the naive one. The time complexity of the order-connected and disconnected algorithms is $\mathcal{O}(N^5)$ on the number of qubits in the Hamiltonian, versus the time complexity of $\mathcal{O}(N^{5.5})$ needed for a naive grouping. Figure 2 b) compares the performance of these three algorithms with three different processors architectures. It shows that the behavior of the non-naive algorithms does not depend on the architecture while the naive one does. This result is important for the practical application of the proposed algorithms on quantum devices with a large number of qubits.

Let us now confront our grouping methods with the previous ones. Table 1 shows the number of groups obtained from the Pauli strings of molecules of sizes between 2 and 16 qubits using different methods: TPB grouping [41], EM grouping [46], and HEEM grouping with the connectivity of the quantum device *ibmq_montreal*. The results of HEEM grouping correspond to the minimum number of groups obtained with any of our three HEEM algorithms in the Monte Carlo study. Table 1 also includes the number of CNOTs required to measure the groups. On the one hand, the HEEM grouping significantly outperforms TPB in terms of the number of groups. On the other hand, the EM grouping has a slightly smaller number of groups than the HEEM but uses a number of CNOTs that grows much more rapidly with the size of the molecules. The number of groups with HEEM scales as $\mathcal{O}(N^{2.45})$ with the number of qubits (the asymptotic scaling values for other magnitudes can be found in the Supplemental Material). Given that both the number of CNOTs, which translates into experimental error, and the number of groups,

which translates into statistical error, are relevant for the final accuracy of the method, the results discussed so far do not completely conclude which is the best grouping method. In order to take both sources of error into account, we have carried out noisy simulations of the energy evaluation of different molecule Hamiltonians and obtained that the HEEM outperforms EM and TPB on average. For example, for CH₄ and a circuit initialized in the GHZ state, the average relative error with TPB is 38.6%, with EM 32.8%, and with HEEM 14.2% (see Supp. Material C). These results can be improved by using error correction and error mitigation methods. However, this topic is beyond the scope of this article.

Finally, to study the performance of HEEM grouping in a practical scenario, we have run noisy simulations and a NISQ experiment of the Variational Quantum Eigensolver (VQE) for the H₂O molecule at its bond distance. We freeze the core and remove an unoccupied orbital to reduce the number of theoretical qubits to 8. Figure 3 a) shows the mean energy per iteration of 240 instances of noisy simulations of VQE using TPB, EM, and HEEM. They were carried out using the noise model and the connectivity of *ibmq_montreal*, provided by IBM-Q [56]. The variational form is composed of 2 layers of local gates and 1 layer of CNOT between the physically connected qubits. The groups used for HEEM correspond to the best groups obtained among the three proposed algorithms. We can see that the grouping scheme with better performance is HEEM, achieving energies below -12.0 Ha after 200 iterations, while neither TPB nor EM reach this value in 300 iterations. This advantage is obtained because HEEM has a lower number of groups than TPB, which reduces the uncertainty of the measurement of the energy, as is explained in [46], and because, unlike EM, it avoids entangled gates between non-physically connected qubits, and hence it avoids noisy, deep circuits. The inset of Fig. 3 a) shows the mean energy in terms of the number of circuits. We can see that the HEEM grouping achieves an energy below -12.0 Ha with about 1200 circuits, while TPB and EM only attain -11.6 Ha and -11.2 Ha, respectively. This means that HEEM allows us to obtain the same results as previous approaches but with fewer circuits. Figure 3 b) shows the experimen-

tal implementation of VQE for the H_2O with TPB, EM, and HEEM. The experiment was carried out on the first 8 qubits of the device *ibmq_guadalupe*. This is a quantum device of 16-qubits, 32 of quantum volume, and 1.245×10^{-2} of average error in the CNOT gates. We can see that the experimental results are in agreement with what was expected from the simulations, that is, HEEM delivers energy lower than TPB and EM at the same number of iterations and using the same number of circuits. The time that each experiment took was 3.8 hours with TPB, 4.4 hours with EM, and 2.7 hours with HEEM. Thus, HEEM provides a speed-up with respect to the other grouping approaches in real hardware.

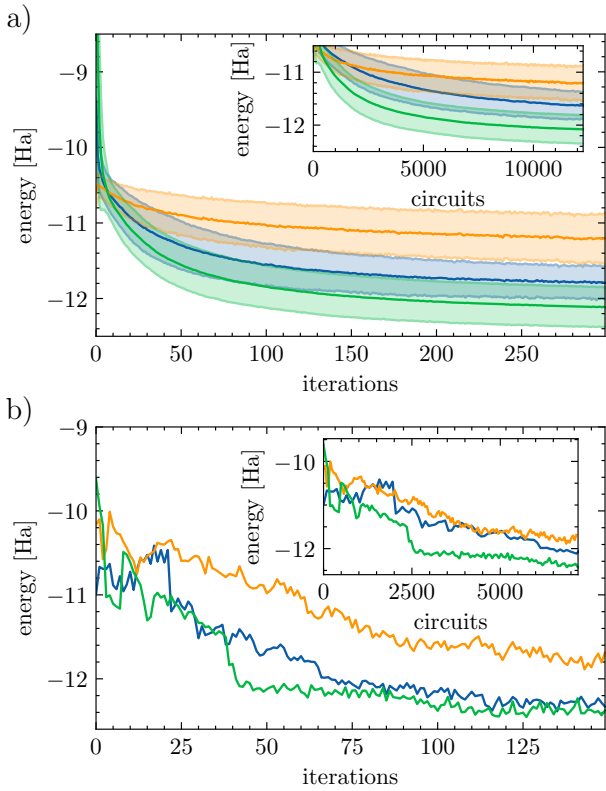


Figure 3: Simulation a), and experimental implementation b), of the VQE for the 8-qubits H_2O Hamiltonian, with a distance of $d = 0.96\text{\AA}$ between hydrogen and oxygen atoms, for TPB in blue, EM in orange, and HEEM in green lines. The simulations were done considering the basis gate, noise model and connectivity of *ibmq_montreal*, while the real experiment is performed in *ibmq_guadalupe*. The classical optimizer used was SPSA with 300 iterations for the simulations and 150 iterations for the experiment. There are 2^{14} shots per circuit in both cases. a) Each point represents 240 independent instances of VQE where the solid lines correspond to the mean energy, and the shaded region to the standard deviation. The exact ground state energy is -13.9 Ha .

4 Conclusions and Outlook

In the NISQ era, in order to achieve the quantum advantage with variational algorithms we need efficient techniques to evaluate the expected values of Hamiltonians. In this article, we have proposed to evaluate Hamiltonians with Hardware Efficient Entangled Measurements (HEEM), measurements that allow one to evaluate simultaneously groups of Pauli Strings, and that employ entangled gates only between qubits that are physically connected on the device. This makes HEEM an efficient alternative for evaluating expected values and speeding up variational algorithms in NISQ devices. Since there are multiple ways to group a set of Pauli strings with HEEM, we have introduced three algorithms to carry out the grouping. The first is the *naive HEEM*, which does not optimize the order of the grouping loops. The other two are *order connected HEEM* and *the order disconnected HEEM*. They optimize the grouping loops by making use of the processor embedding problem, the problem of finding the optimal map of the theoretical qubits into the physical qubits, as it is shown in Fig. 1.

We compare our methods and conclude that the order connected and order disconnected algorithms outperform the naive algorithm on average number of groups and time execution. Our methods improve previous works. HEEM uses less groups than TPB [41], with only a slight increase in the number of required CNOTs. Also, HEEM requires less CNOTs than EM [46], using only a few more groups. The number of groups quantifies the statistical error, while the number of CNOTs quantifies the experimental error. Taking both sources of error into account, HEEM outperforms both TPB and EM. We have shown, with noisy simulations and experiments, that HEEM achieves better results with the same number of circuits and is experimentally faster than TPB and EM in practical scenarios, such as finding the ground state energy of H_2O with VQE.

Several extensions can be incorporated into our proposal. The grouping of Pauli strings by HEEM can be improved by considering entanglement between a larger number of qubits. This would allow to further reduce the number of groups at the expense of more entanglement resources, which could be an intermediate step towards EM grouping as the quality of the entangling gates improves. The method can also be refined by including the error of the CNOT gates of the chip as weights in the graph that represents the connectivity of the chip. This would produce better results by ensuring that the majority of the entangling operations are performed over pairs of qubits with the least CNOT gate errors. Furthermore, we can implement ideas from previous methods to HEEM. Given that the number of groups and CNOTs are proxies for the error of the measurement, we can explore the

behaviour of HEEM under more elaborated metrics, such as the proposed in [47]. In the same article it is also suggested to sort the Pauli strings according to their weights in the Hamiltonian, which could improve HEEM in practical scenarios.

HEEM grouping is useful not only in variational algorithms, but also in any task that requires the evaluation of several Pauli strings, such as full quantum tomography [57, 58], compressed sensing [59, 60], reduced density matrix tomography [32, 33], classical shadows [29, 30], or direct fidelity estimation [61, 62]. The processor embedding problem also has applications in other branches of quantum information, such as the physical layout problem, and even in the industry: suppose that a country has to decide in which cities it locates different parts of an industrial process. Then, the roadmap of a country can be interpreted as the connectivity of the chip, while the affinity of different parts of the industrial process can be regarded as the compatibility of the theoretical qubits.

The code to reproduce the algorithms and the figures of this article can be found in [63].

5 Acknowledgements

We thank Juan José García-Ripoll for valuable feedback on the manuscript. This work has been supported by funding from Spanish project PGC2018-094792-B-I00 (MCIU/AEI/FEDER, UE) and CAM/FEDER Project No. S2018/TCS-4342 (QUITEMAD-CM). G. F. P. and G. J. acknowledge support from the European Union’s Horizon 2020 FET-Open project SuperQuLAN (899354). F.E.G. was supported by a Marie Skłodowska-Curie Action from the EC (COFUND grant no. 945045), and by the NWO Gravitation project NETWORKS (grant no. 024.002.003). D.F.F. acknowledges support from the FPU Program No. FPU20/04762. L.P. was supported by ANID-PFCHA/DOCTORADO-BECAS-CHILE/2019-77220027. We thank the IBM Quantum Team for making multiple devices available to the CSIC-IBM Quantum Hub via the IBM Quantum Experience. The views expressed are those of the authors, and do not reflect the official policy or position of IBM or the IBM Quantum team.

References

- [1] John Preskill. Quantum computing in the NISQ era and beyond. *Quantum*, 2:79, August 2018. DOI: 10.22331/q-2018-08-06-79.
- [2] Ilya G. Ryabinkin, Scott N. Genin, and Artur F. Izmaylov. Constrained variational quantum eigensolver: Quantum computer search engine in the fock space. *Journal of Chemical Theory and Computation*, 15:249–255, 1 2018. DOI: 10.1021/ACS.JCTC.8B00943.
- [3] Jonathan Romero, Ryan Babbush, Jarrod R McClean, Cornelius Hempel, Peter J Love, and Alán Aspuru-Guzik. Strategies for quantum computing molecular energies using the unitary coupled cluster ansatz. *Quantum Science and Technology*, 4:014008, 10 2018. ISSN 2058-9565. DOI: 10.1088/2058-9565/AAD3E4.
- [4] Ilya G. Ryabinkin, Tzu-Ching Yen, Scott N. Genin, and Artur F. Izmaylov. Qubit coupled cluster method: A systematic approach to quantum chemistry on a quantum computer. *Journal of Chemical Theory and Computation*, 14:6317–6326, 12 2018. DOI: 10.1021/ACS.JCTC.8B00932.
- [5] William Kirby, Bryce Fuller, Charles Hadfield, and Antonio Mezzacapo. Second-quantized fermionic hamiltonians for quantum simulation with polylogarithmic qubit and gate complexity, September 2021. URL <http://arxiv.org/abs/2109.14465>.
- [6] Kishor Bharti, Alba Cervera-Lierta, Thi Ha Kyaw, Tobias Haug, Sumner Alperin-Lea, Abhinav Anand, Matthias Degroote, Hermanni Heimonen, Jakob S. Kottmann, Tim Menke, Wai-Keong Mok, Sukin Sim, Leong-Chuan Kwek, and Alán Aspuru-Guzik. Noisy intermediate-scale quantum (nisq) algorithms, January 2021. URL <http://arxiv.org/abs/2101.08448>.
- [7] Jules Tilly, Hongxiang Chen, Shuxiang Cao, Dario Picozzi, Kanav Setia, Ying Li, Edward Grant, Leonard Woessnig, Ivan Rungger, George H. Booth, and Jonathan Tennyson. The variational quantum eigensolver: a review of methods and best practices, November 2021. URL <http://arxiv.org/abs/2111.05176>.
- [8] Artur F. Izmaylov, Tzu-Ching Yen, and Ilya G. Ryabinkin. Revising the measurement process in the variational quantum eigensolver: is it possible to reduce the number of separately measured operators? *Chemical Science*, 10: 3746–3755, 2019. ISSN 2041-6520. DOI: 10.1039/C8SC05592K.
- [9] Alberto Peruzzo, Jarrod McClean, Peter Shadbolt, Man-Hong Yung, Xiao-Qi Zhou, Peter J. Love, Alán Aspuru-Guzik, and Jeremy L. O’Brien. A variational eigenvalue solver on a photonic quantum processor. *Nature Communications*, 5(1), July 2014. DOI: 10.1038/ncomms5213.
- [10] Edward Farhi, Jeffrey Goldstone, and Sam Gutmann. A quantum approximate optimization algorithm, November 2014. URL <http://arxiv.org/abs/1411.4028>.
- [11] Nikolaj Moll, Panagiotis Barkoutsos, Lev S Bishop, Jerry M Chow, Andrew Cross, Daniel J Egger, Stefan Filipp, Andreas Fuhrer, Jay M Gambetta, Marc Ganzhorn, Abhinav Kandala, Antonio Mezzacapo, Peter Müller, Walter Riess,

Gian Salis, John Smolin, Ivano Tavernelli, and Kristan Temme. Quantum optimization using variational algorithms on near-term quantum devices. *Quantum Science and Technology*, 3:030503, 6 2018. ISSN 2058-9565. DOI: 10.1088/2058-9565/AAB822.

[12] Abhinav Kandala, Antonio Mezzacapo, Kristan Temme, Maika Takita, Markus Brink, Jerry M. Chow, and Jay M. Gambetta. Hardware-efficient variational quantum eigensolver for small molecules and quantum magnets. *Nature*, 549(7671):242–246, September 2017. DOI: 10.1038/nature23879.

[13] Cornelius Hempel, Christine Maier, Jonathan Romero, Jarrod McClean, Thomas Monz, Heng Shen, Petar Jurcevic, Ben P. Lanyon, Peter Love, Ryan Babbush, Alán Aspuru-Guzik, Rainer Blatt, and Christian F. Roos. Quantum chemistry calculations on a trapped-ion quantum simulator. *Physical Review X*, 8, 7 2018. ISSN 21603308. DOI: 10.1103/PhysRevX.8.031022.

[14] Yunseong Nam, Jwo Sy Chen, Neal C. Pisenti, Kenneth Wright, Conor Delaney, Dmitri Maslov, Kenneth R. Brown, Stewart Allen, Jason M. Amini, Joel Apisdorf, Kristin M. Beck, Aleksey Blinov, Vandiver Chaplin, Mika Chmielewski, Coleman Collins, Shantanu Debnath, Kai M. Hudek, Andrew M. Ducore, Matthew Keesan, Sarah M. Kreikemeier, Jonathan Mizrahi, Phil Solomon, Mike Williams, Jaime David Wong-Campos, David Moehring, Christopher Monroe, and Jungsang Kim. Ground-state energy estimation of the water molecule on a trapped-ion quantum computer. *npj Quantum Information*, 6, 12 2020. ISSN 20566387. DOI: 10.1038/s41534-020-0259-3.

[15] Daniel J. Egger, Claudio Gambella, Jakub Marecek, Scott McFaddin, Martin Mevissen, Rudy Raymond, Andrea Simonetto, Stefan Woerner, and Elena Yndurain. Quantum computing for finance: State-of-the-art and future prospects. *IEEE Transactions on Quantum Engineering*, 1: 1–24, 2020. DOI: 10.1109/TQE.2020.3030314.

[16] Pontus Vikstål, Mattias Grönkvist, Marika Svensson, Martin Andersson, Göran Johansson, and Giulia Ferrini. Applying the quantum approximate optimization algorithm to the tail-assignment problem. *Physical Review Applied*, 14:1–11, 2020. ISSN 23317019. DOI: 10.1103/PhysRevApplied.14.034009.

[17] Florian Neukart, Gabriele Compostella, Christian Seidel, David von Dollen, Sheir Yarkoni, and Bob Parney. Traffic flow optimization using a quantum annealer. *Frontiers in ICT*, 4:29, 12 2017. ISSN 2297-198X. DOI: 10.3389/fict.2017.00029.

[18] Jacob Biamonte, Peter Wittek, Nicola Pancotti, Patrick Rebentrost, Nathan Wiebe, and Seth Lloyd. Quantum machine learning. *Nature*, 549:195–202, 9 2017. ISSN 0028-0836. DOI: 10.1038/nature23474.

[19] Marcello Benedetti, Edward Grant, Leonard Wossnig, and Simone Severini. Adversarial quantum circuit learning for pure state approximation. *New Journal of Physics*, 21, 4 2019. ISSN 13672630. DOI: 10.1088/1367-2630/ab14b5.

[20] Andrew Patterson, Hongxiang Chen, Leonard Wossnig, Simone Severini, Dan Browne, and Ivan Rungger. Quantum state discrimination using noisy quantum neural networks. *Physical Review Research*, 3:013063, 1 2021. ISSN 2643-1564. DOI: 10.1103/PhysRevResearch.3.013063.

[21] H. Chen, L. Wossnig, S. Severini, H. Neven, and M. Mohseni. Universal discriminative quantum neural networks. *Quantum Machine Intelligence*, 3, 6 2021. ISSN 2524-4906. DOI: 10.1007/s42484-020-00025-7.

[22] Xin Wang, Zhixin Song, and Youle Wang. Variational quantum singular value decomposition. *Quantum*, 5:483, 6 2021. ISSN 2521-327X. DOI: 10.22331/q-2021-06-29-483.

[23] Kun Wang, Zhixin Song, Xuanqiang Zhao, Zihe Wang, and Xin Wang. Detecting and quantifying entanglement on near-term quantum devices, December 2020. URL <http://arxiv.org/abs/2012.14311>.

[24] A. D. Muñoz-Moller, L. Pereira, L. Zambrano, J. Cortés-Vega, and A. Delgado. Variational determination of multi-qubit geometrical entanglement in nisq computers, October 2021. URL <https://arxiv.org/abs/2110.03709>.

[25] Xiao Yuan, Suguru Endo, Qi Zhao, Ying Li, and Simon C. Benjamin. Theory of variational quantum simulation. *Quantum*, 3:191, October 2019. DOI: 10.22331/q-2019-10-07-191.

[26] Tyson Jones, Suguru Endo, Sam McArdle, Xiao Yuan, and Simon C. Benjamin. Variational quantum algorithms for discovering hamiltonian spectra. *Physical Review A*, 99(6), June 2019. DOI: 10.1103/physreva.99.062304.

[27] Paula García-Molina, Javier Rodríguez-Mediavilla, and Juan José García-Ripoll. Quantum fourier analysis for multivariate functions and applications to a class of schrödinger-type partial differential equations. *Physical Review A*, 105(1):012433, jan 2022. DOI: 10.1103/physreva.105.012433.

[28] Pranav Gokhale, Olivia Angiuli, Yongshan Ding, Kaiwen Gui, Teague Tomesh, Martin Suchara, Margaret Martonosi, and Frederic T Chong. Minimizing state preparations in variational quantum eigensolver by partitioning into commuting families, July 2019. URL <https://arxiv.org/abs/1907.13623>.

[29] Hsin Yuan Huang, Richard Kueng, and John Preskill. Predicting many properties of a quan-

tum system from very few measurements. *Nature Physics*, 16:1050–1057, 10 2020. ISSN 17452481. DOI: 10.1038/s41567-020-0932-7.

[30] Senrui Chen, Wenjun Yu, Pei Zeng, and Steven T. Flammia. Robust shadow estimation. *PRX Quantum*, 2, 9 2021. DOI: 10.1103/prxquantum.2.030348.

[31] Scott Aaronson. Shadow tomography of quantum states. *SIAM Journal on Computing*, 49(5):STOC18–368–STOC18–394, January 2020. DOI: 10.1137/18m120275x.

[32] Jordan Cotler and Frank Wilczek. Quantum overlapping tomography. *Physical Review Letters*, 124:100401, 3 2020. ISSN 0031-9007. DOI: 10.1103/PhysRevLett.124.100401.

[33] Xavier Bonet-Monroig, Ryan Babbush, and Thomas E. O’Brien. Nearly optimal measurement scheduling for partial tomography of quantum states. *Phys. Rev. X*, 10:031064, Sep 2020. DOI: 10.1103/PhysRevX.10.031064.

[34] Roger G. Melko, Giuseppe Carleo, Juan Carrasquilla, and J. Ignacio Cirac. Restricted boltzmann machines in quantum physics. *Nature Physics*, 15:887–892, 9 2019. ISSN 1745-2473. DOI: 10.1038/s41567-019-0545-1.

[35] Giacomo Torlai, Guglielmo Mazzola, Giuseppe Carleo, and Antonio Mezzacapo. Precise measurement of quantum observables with neural-network estimators. *Physical Review Research*, 2:022060, 6 2020. ISSN 2643-1564. DOI: 10.1103/PhysRevResearch.2.022060.

[36] Ariel Shlosberg, Andrew J. Jena, Priyanka Mukhopadhyay, Jan F. Haase, Felix Leditzky, and Luca Dellantonio. Adaptive estimation of quantum observables, October 2021. URL <http://arxiv.org/abs/2110.15339>.

[37] Harish J. Vallury, Michael A. Jones, Charles D. Hill, and Lloyd C. L. Hollenberg. Quantum computed moments correction to variational estimates. *Quantum*, 4:373, December 2020. DOI: 10.22331/q-2020-12-15-373. URL <https://doi.org/10.22331/q-2020-12-15-373>.

[38] Nicholas C Rubin, Ryan Babbush, and Jarrod McClean. Application of fermionic marginal constraints to hybrid quantum algorithms. *New Journal of Physics*, 20(5):053020, May 2018. DOI: 10.1088/1367-2630/aab919. URL <https://doi.org/10.1088/1367-2630/aab919>.

[39] Jarrod R. McClean, Jonathan Romero, Ryan Babbush, and Alán Aspuru-Guzik. The theory of variational hybrid quantum-classical algorithms. *New Journal of Physics*, 18, 2 2016. ISSN 13672630. DOI: 10.1088/1367-2630/18/2/023023.

[40] Andrew Arrasmith, Lukasz Cincio, Rolando D. Somma, and Patrick J. Coles. Operator sampling for shot-frugal optimization in variational algo-

rithms, 2020. URL <https://arxiv.org/abs/2004.06252v1>.

[41] Sergey Bravyi, Jay M. Gambetta, Antonio Mezzacapo, and Kristan Temme. Tapering off qubits to simulate fermionic hamiltonians, January 2017. URL <http://arxiv.org/abs/1701.08213>.

[42] Tzu-Ching Yen, Vladyslav Verteletskyi, and Artur F. Izmaylov. Measuring all compatible operators in one series of a single-qubit measurements using unitary transformations, 2020. URL <http://arxiv.org/abs/1907.09386>.

[43] Vladyslav Verteletskyi, Tzu-Ching Yen, and Artur F. Izmaylov. Measurement optimization in the variational quantum eigensolver using a minimum clique cover. *The Journal of Chemical Physics*, 152(12):124114, March 2020. DOI: 10.1063/1.5141458.

[44] Ruho Kondo, Yuki Sato, Satoshi Koide, Seiji Kajita, and Hideki Takamatsu. Computationally efficient quantum expectation with extended bell measurements, October 2021. URL <http://arxiv.org/abs/2110.09735>.

[45] Artur F. Izmaylov, Tzu-Ching Yen, Robert A. Lang, and Vladyslav Verteletskyi. Unitary partitioning approach to the measurement problem in the variational quantum eigensolver method. *Journal of Chemical Theory and Computation*, 16(1):190–195, 2020. DOI: 10.1021/acs.jctc.9b00791.

[46] Ikko Hamamura and Takashi Imamichi. Efficient evaluation of quantum observables using entangled measurements. *npj Quantum Information*, 6 (1), June 2020. DOI: 10.1038/s41534-020-0284-2.

[47] Ophelia Crawford, Barnaby van Straaten, Daochen Wang, Thomas Parks, Earl Campbell, and Stephen Brierley. Efficient quantum measurement of pauli operators in the presence of finite sampling error. *Quantum*, 5:385, January 2021. DOI: 10.22331/q-2021-01-20-385.

[48] Andrew Zhao, Andrew Tranter, William M. Kirby, Shu Fay Ung, Akimasa Miyake, and Peter J. Love. Measurement reduction in variational quantum algorithms. *Physical Review A*, 101(6), June 2020. DOI: 10.1103/physreva.101.062322.

[49] Andrew Jena, Scott Genin, and Michele Mosca. Pauli partitioning with respect to gate sets, July 2019. URL <https://arxiv.org/abs/1907.07859>.

[50] Piotr Formanowicz and Krzysztof Tanaś. A survey of graph coloring - its types, methods and applications. *Foundations of Computing and Decision Sciences*, 37, 09 2012. DOI: 10.2478/v10209-011-0012-y.

[51] Richard M. Karp. Reducibility among combinatorial problems. In *Complexity of Computer*

Computations, pages 85–103. Springer US, 1972. DOI: 10.1007/978-1-4684-2001-2_9.

[52] Pasin Manurangsi. Almost-polynomial ratio eth-hardness of approximating densest k -subgraph, 11 2016. URL <http://arxiv.org/abs/1611.05991>.

[53] Renata Sotirov. On solving the densest k -subgraph problem on large graphs, 1 2019. URL <http://arxiv.org/abs/1901.06344>.

[54] Cédric Avanthay, Alain Hertz, and Nicolas Zufferey. A variable neighborhood search for graph coloring. *European Journal of Operational Research*, 151:379–388, 12 2003. DOI: 10.1016/S0377-2217(02)00832-9.

[55] Bochen Tan and Jason Cong. Optimal layout synthesis for quantum computing. In *Proceedings of the 39th International Conference on Computer-Aided Design*. ACM, November 2020. DOI: 10.1145/3400302.3415620.

[56] IBM Quantum Computing, 2022. URL <https://quantum-computing.ibm.com/>.

[57] Daniel F. V. James, Paul G. Kwiat, William J. Munro, and Andrew G. White. Measurement of qubits. *Phys. Rev. A*, 64:052312, Oct 2001. DOI: 10.1103/PhysRevA.64.052312. URL <https://link.aps.org/doi/10.1103/PhysRevA.64.052312>.

[58] H. Häffner, W. Hänsel, C. F. Roos, J. Benhelm, D. Chek al kar, M. Chwalla, T. Körber, U. D. Rapol, M. Riebe, P. O. Schmidt, C. Becher, O. Gühne, W. Dür, and R. Blatt. Scalable multiparticle entanglement of trapped ions. *Nature*, 438(7068):643–646, December 2005. DOI: 10.1038/nature04279. URL <https://doi.org/10.1038/nature04279>.

[59] David Gross, Yi-Kai Liu, Steven T. Flammia, Stephen Becker, and Jens Eisert. Quantum state tomography via compressed sensing. *Phys. Rev. Lett.*, 105:150401, Oct 2010. DOI: 10.1103/PhysRevLett.105.150401. URL <https://link.aps.org/doi/10.1103/PhysRevLett.105.150401>.

[60] C. A. Riofrío, D. Gross, S. T. Flammia, T. Monz, D. Nigg, R. Blatt, and J. Eisert. Experimental quantum compressed sensing for a seven-qubit system. *Nature Communications*, 8(1):15305, May 2017. DOI: 10.1038/ncomms15305. URL <https://doi.org/10.1038/ncomms15305>.

[61] Steven T. Flammia and Yi-Kai Liu. Direct fidelity estimation from few pauli measurements. *Phys. Rev. Lett.*, 106:230501, Jun 2011. DOI: 10.1103/PhysRevLett.106.230501. URL <https://link.aps.org/doi/10.1103/PhysRevLett.106.230501>.

[62] Marcus P. da Silva, Olivier Landon-Cardinal, and David Poulin. Practical characterization of quantum devices without tomography. *Phys. Rev. Lett.*, 107:210404, Nov 2011. DOI: 10.1103/PhysRevLett.107.210404. URL <https://link.aps.org/doi/10.1103/PhysRevLett.107.210404>.

[63] Francisco Escudero, David Fernández-Fernández, Gabriel Jaumà, Guillermo F. Peñas, and Luciano Pereira. Hardware efficient variational quantum eigensolver with entangled measurements: Code repository, February 2022. URL <https://doi.org/10.5281/zenodo.6074767>.

Supplemental Material

Hardware-efficient entangled measurements for variational quantum algorithms

Francisco Escudero,^{1,2} David Fernández-Fernández,^{1,3}, Gabriel Jaumà,¹ Guillermo F. Peñas,¹ Luciano Pereira¹

¹*Instituto de Física Fundamental, IFF-CSIC, Calle Serrano 113b, 28006 Madrid, Spain*

²*Networks, Qusoft and CWI, Amsterdam, Netherlands.*

³*Instituto de Ciencia de Materiales de Madrid, ICMM-CSIC, E-28049 Madrid, Spain*

A Algorithms

In this appendix the heuristic algorithms announced in the main text are provided and motivated in more detail. All of them have been implemented in a library compatible with QISKit [63].

A.1 Taking chip's connectivity into account

Herewith we expose the modification made to the algorithm in [46] needed to take into account chip's connectivity. This modification is the inclusion of the line 8 in the Algorithm 2.

In addition, we explain why this algorithm depends on the orders of the iterative elements, as announced in section 2. The line 8 of Algorithm 2 shows that this algorithm depends on the processor embedding map chosen (in this version of the algorithm τ is implicitly chosen to be $\tau(i) = i$ for all $i \in \{0, \dots, N - 1\}$). Line 6 of Algorithm 2 shows the dependence on the order used to run through the assignable measurements. Line 7 of Algorithm 2 shows the dependence in the order of the qubits. Finally, lines 4 and 9 of Algorithm 1 show that the algorithm depends on the order of the Pauli strings (in this version of the algorithm, the Pauli string order is chosen to be the largest-degree-first). In the Subsection A.2 we provide heuristic algorithms to choose these orders adequately.

Algorithm 1: Greedy grouping taking chip's connectivity into account

Data: A set of n Pauli strings PS of N qubits, a set of measurements $\mathcal{E} = \{\mathcal{E}_1, \dots, \mathcal{E}_l\}$ and a topology graph $G = (V, E)$

1 Build the Pauli Graph of PS; let $\{v_i\}_{i=1}^n$ be its vertices;
2 Initialize the measurements M ;
3 Initialize the groups Gr ;
4 **for** $i=1, \dots, n$ **do**
5 **if** v_i is not in any group **then**
6 Initialize measurement M_i and assign M_i to v_i ;
7 Initialize the group Gr_i and add v_i to Gr_i ;
8 *# M_i stores a set of local measurements, indicating in which qubits they act, such that are compatible with all Pauli Strings in group Gr_i ;*
9 **for** $j=i+1, \dots, n$ **do**
10 **if** v_j is not in any group **then**
11 **if** v_i and v_j are jointly measurable with respect to M_i , \mathcal{E} and G (see algorithm 2) **then**
12 Update M_i and add v_j to Gr_i ;
13 Append M_i to M and Gr_i to Gr ;
14 **return** M, Gr

Algorithm 2: Greedy measurement assignment taking chip's connectivity into account

Data: Two Pauli strings v_i and v_j , a set of measurements $\mathcal{E} = \{\mathcal{E}_1, \dots, \mathcal{E}_l\}$, a topology graph $G = (V, E)$, a current assignment of a measurement M_i

1 **if** v_j is not compatible with M_i **then**
2 **return** *fail*;
3 Let U be the indices of qubits without an assigned local measurement in M_i ;
4 Remove from U the indices where v_i and v_j coincide;
5 **while** $U \neq \emptyset$ **do**
6 **for** $\mathcal{E} \in \mathcal{E}$ **do**
7 **for** $p \in \text{permutations of } U \text{ of size equal to the number of qubits where } \mathcal{E} \text{ acts}$ **do**
8 **if** the qubits of p are in E (only do if p has size bigger than 1) **then**
9 **if** v_i and v_j are compatible with \mathcal{E} in the qubits at position p **then**
10 Update M_i with \mathcal{E} at position p ;
11 Remove the qubits of p from U ;
12 Go to line 5;
13 **return** *fail*
14 **return** *success, M_i*

A.2 processor embedding and order algorithms

In this section we provide heuristic algorithms to propose adequate orders to the iterative items of Algorithms 1 and 2. In particular, we provide a heuristic algorithm for the processor embedding problem. For further detail about these concepts, see Subsections 2.1 and A.1. Algorithm 3 computes the compatibility matrix. Algorithm 4 proposes a processor embedding map that aims to map the pair of theoretical qubits (i, j) with highest entries C_{ij} to physically connected qubits. Algorithm 5 does the same as Algorithm 4 with the additional requirement of ensuring that the graph G' is connected once is mapped to G through τ , i.e., $\tau(G')$ is a connected sub-graph of G . Although Algorithm 5 may look like an arbitrary modification of Algorithm 4, results show that the performance is improved when imposing that $\tau(G')$ is connected (see Figure 2). Finally, Algorithm 6 outputs the τ -compatibility matrix C^τ and the dictionaries CM^τ and CQ^τ .

Algorithm 3: Construction of compatibility matrix

Data: A set of n Pauli strings PS of N qubits

1 Initialize C as an $N \times N$ as a matrix of -1's;
2 **for** $i \in \{0, \dots, N - 1\}$ **do**
3 **for** $j \in \{i + 1, \dots, N - 1\}$ **do**
4 $PS' = PS[:, [i, j]]$;
5 Create a dictionary $F = \{(II, FII), (IX, FIX), \dots, (ZZ, FZZ)\}$ with FII being the number of factors II appearing in $PS' \dots$;
6 $CMBell_{ij} = \frac{[F(II) + F(XX) + F(YY) + F(ZZ)]^2 - [F(II) + F(XX) + F(YY) + F(ZZ)]}{2}$;
7 $CM\chi_{ij} = \dots$;
8 $C[i, j] = C[j, i] = CMBell_{ij} + CM\chi_{ij} + CM\tilde{\chi}_{ij} + CM\Omega_{ij}^X + CM\Omega_{ij}^Y + CM\Omega_{ij}^Z$;
9 **return** C

Algorithm 4: Processor embedding map construction

Data: A compatibility matrix C and a topology graph $G = (V, E)$

- 1 Initialize a list $AQ = []$; *# It stores the theoretical qubits qith an assigned physical qubit.*
- 2 Initialize a list $\tau = []$; *# It stores the information of the processor embedding map.*
- 3 **while** $AQ \neq \{1, \dots, N - 1\}$ **do**
- 4 Choose (i_0, j_0) such that $C_{i_0, j_0} = \max_{ij} C_{ij}$;
- 5 **if** $i_0 \in AQ$ **and** $j_0 \in AQ$ **then**
- 6 $C[j_0, i_0] = C[i_0, j_0] = -1$
- 7 **else if** $i_0 \in AQ$ **or** $j_0 \in AQ$ **then**
- 8 *#Suppose that $i_0 \in AQ$. i_0 and j_0 cannot simultaneously belong to AQ;*
- 9 Let J be not assigned neighbor of $\tau(i_0)$;
- 10 Append (j_0, J) to τ (so $\tau(j_0) = J$);
- 11 Append j_0 to AQ ;
- 12 $C[i_0, j_0] = C[j_0, i_0] = -1$;
- 13 **for** $S \in \text{neighbors of } \tau(j_0)$ **do**
- 14 **if** S is assigned to a theoretical qubit **then**
- 15 $E = E - (S, \tau(j_0))$;
- 16 **if** $\text{degree}(S) == 0$ **then**
- 17 s=theoretical qubit assigned to the physical qubit S ;
- 18 $C[s, :] = C[:, s] = -1$;
- 19 **if** $\text{degree}(\tau(j_0)) == 0$ **then**
- 20 $C[j_0, :] = C[:, j_0] = -1$
- 21 *# Note that $\text{degree}(\tau(i_0))=0$ means that the physical qubit correspondent to the theoretical qubit i_0 has no available neighbors (because we update the connectivity graph by deleting the edges corresponding to pairs of physical qubits that have been assigned). Setting $C[i_0, :]$ and $C[:, i_0]$ to -1 ensures that no pair containing i_0 will be chosen at the beginning of the while. By doing that we decrease the number of iterations inside the while.*
- 22 **else**
- 23 **if** there is a pair of unassigned and connected physical qubits **then**
- 24 Append (j_0, J) and (i_0, I) to τ (so $\tau(i_0) = I$ and $\tau(j_0) = J$);
- 25 Append i_0 and j_0 to AQ ;
- 26 $C[i_0, j_0] = C[j_0, i_0] = -1$;
- 27 **for** $S \in \text{neighbors of } \tau(i_0)$ **do**
- 28 **if** S is assigned to a theoretical qubit **then**
- 29 $E = E - (S, \tau(i_0))$;
- 30 **if** $\text{degree}(S) == 0$ **then**
- 31 s=theoretical qubit assigned to the physical qubit S ;
- 32 $C[s, :] = C[:, s] = -1$;
- 33 **for** $S \in \text{neighbors of } \tau(j_0)$ **do**
- 34 **if** S is assigned to a theoretical qubit **then**
- 35 $E = E - (S, \tau(j_0))$;
- 36 **if** $\text{degree}(S) == 0$ **then**
- 37 s=theoretical qubit assigned to the physical qubit S ;
- 38 $C[s, :] = C[:, s] = -1$;
- 39 **if** $\text{degree}(\tau(i_0)) == 0$ **then**
- 40 $C[i_0, :] = C[:, i_0] = -1$;
- 41 **else**
- 42 $C[i_0, j_0] = C[j_0, i_0] = -1$

43 **return** τ

Algorithm 5: Processor embedding map construction, ensuring that $\tau(G')$ is connected

Data: A compatibility matrix C and a topology graph $G = (V, E)$

1 Initialize a list $AQ = []$; *# It stores the theoretical qubits with an assigned physical qubit.*

2 Initialize a list $\tau = []$; *# It stores the information of the processor embedding map.*

3 Choose (i_0, j_0) such that $C_{i_0 j_0} = \max_{ij} C_{ij}$;

4 Let (I, J) be a pair of physically connected qubits;

5 Append (j_0, J) and (i_0, I) to τ ;

6 Append i_0 and j_0 to AQ ;

7 $C[i_0, j_0] = C[j_0, i_0] = -1$;

8 $E = E - (\tau(i_0), \tau(j_0))$;

9 **if** $\text{degree}(\tau(i_0)) == 0$ **then**

10 $C[i_0, :] = C[:, i_0] = -1$

11 **if** $\text{degree}(\tau(j_0)) == 0$ **then**

12 $C[j_0, :] = C[:, j_0] = -1$

13 **while** $AQ \neq \{1, \dots, N - 1\}$ **do**

14 $C' = C[AQ, :]$;

15 Choose (i_0, j_0) such that $C'_{i_0, j_0} = \max_{ij} C'_{ij}$;

16 **if** $i_0 \in AQ$ **and** $j_0 \in AQ$ **then**

17 $C[j_0, i_0] = C[i_0, j_0] = -1$

18 **else if** $i_0 \in AQ$ **or** $j_0 \in AQ$ **then**

19 *#Suppose that $i_0 \in AQ$. i_0 and j_0 cannot simultaneously belong to AQ ;*

20 Let J be not assigned neighbor of $\tau(i_0)$;

21 Append (j_0, J) to τ (so $\tau(j_0) = J$);

22 Append j_0 to AQ ;

23 $C[i_0, j_0] = C[j_0, i_0] = -1$;

24 **for** $S \in \text{neighbors of } \tau(j_0)$ **do**

25 **if** S is assigned to a theoretical qubit **then**

26 $E = E - (S, \tau(j_0))$;

27 **if** $\text{degree}(S) == 0$ **then**

28 s=theoretical qubit assigned to the physical qubit S ;

29 $C[s, :] = C[:, s] = -1$;

30 **if** $\text{degree}(\tau(j_0)) == 0$ **then**

31 $C[j_0, :] = C[:, j_0] = -1$

32 *# Note that $\text{degree}(\tau(i_0))=0$ means that the physical qubit correspondent to the theoretical qubit i_0 has no available neighbors (because we update the connectivity graph by deleting the edges corresponding to pairs of physical qubits that have been assigned). Setting $C[i_0, :]$ and $C[:, i_0]$ to -1 ensures that no pair containing i_0 will be chosen at the beginning of the while. By doing that we decrease the number of iterations inside the while.*

33 **return** τ

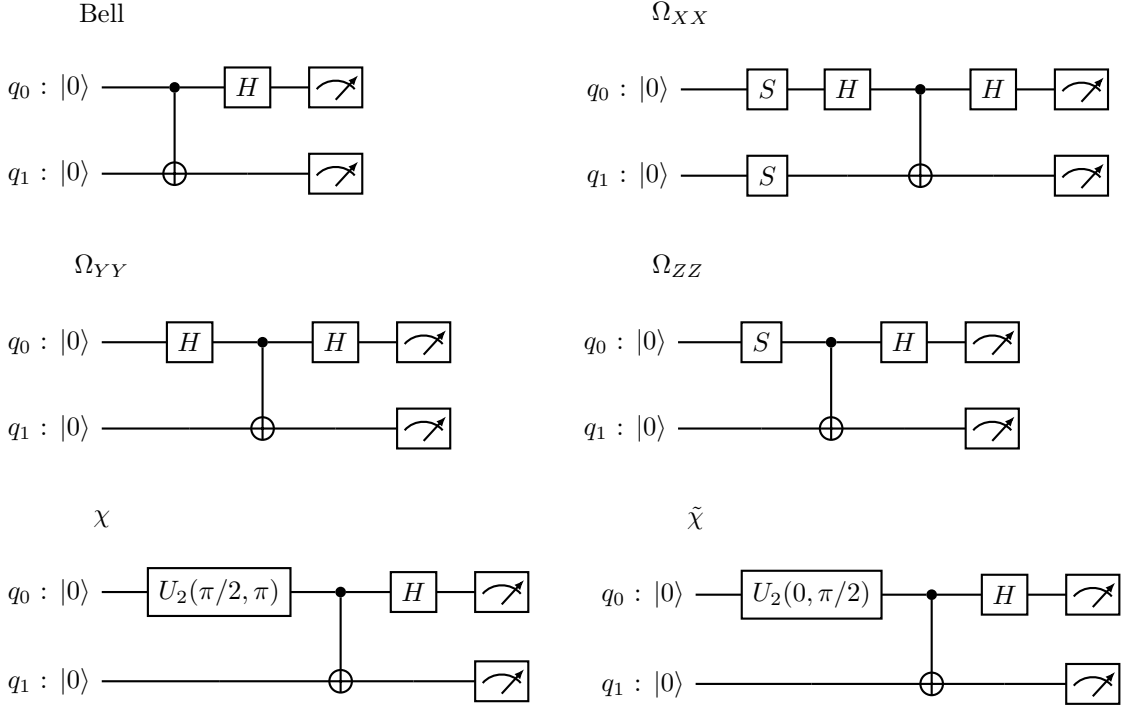
Algorithm 6: Construction of τ -compatibility matrix

Data: A set of n Pauli strings PS of N qubits, a processor embedding map τ and a topology graph $G = (V, E)$

- 1 Initialize C^τ as an $N \times N$ matrix of -1's;
- 2 Initialize CM^τ as a dictionary $CM^\tau = \{(\mathcal{X}, 0), (\mathcal{Y}, 0), (\mathcal{Z}, 0), (Bell, 0), (\chi, 0), (\tilde{\chi}, 0), (\Omega^X, 0), (\Omega^Y, 0), (\Omega^Z, 0)\}$;
- 3 Initialize CQ^τ as a zeros array of length N ;
- 4 **for** $i \in \{0, \dots, N - 1\}$ **do**
- 5 **for** $j \in \{i + 1, \dots, N - 1\}$ **do**
- 6 **if** $(\tau(i), \tau(j)) \in E$ **then**
- 7 $PS' = PS[:, [i, j]]$;
- 8 Build a dictionary $F = \{(II, FII), (IX, FIX), \dots, (ZZ, FZZ)\}$ with FII being the number of factors II appearing in $PS' \dots$;
- 9 $C^T Bell_{ij} = \frac{[F(II) + F(XX) + F(YY) + F(ZZ)]^2 - [F(II) + F(XX) + F(YY) + F(ZZ)]}{2}$;
- 10 $C^\tau \chi_{ij} = \dots$;
- 11 $C^\tau [i, j] = C^\tau [j, i] = C^T Bell_{ij} + C^\tau \chi_{ij} + C^\tau \tilde{\chi}_{ij} + C^\tau \Omega_{ij}^X + C^\tau \Omega_{ij}^Y + C^\tau \Omega_{ij}^Z$;
- 12 $C^T Bell = C^T Bell + C^T Bell_{ij}$, $C^\tau \chi = \dots$;
- 13 $CQ^\tau [i] = CQ^\tau [i] + C^\tau [i, j]$;
- 14 $CQ^\tau [j] = CQ^\tau [j] + C^\tau [i, j]$;
- 15 Build a dictionary $F = \{(I, FI), (X, FX), (Y, FY), (Z, FZ)\}$ with FI being the number of factors I appearing in $PS[:, i] \dots$;
- 16 **for** $m \in \{\mathcal{X}, \mathcal{Y}, \mathcal{Z}\}$ **do**
- 17 $C^T m_i = \binom{FI + Fm}{2}$;
- 18 $CQ^\tau [i] = CQ^\tau [i] + C^T m_i$;
- 19 $C^T m = C^T m + C^T m_i$;
- 20 **return** C^τ, CM^τ, CQ^τ

B Entangled measurements

We have identified the relevant two-qubit entangled measurements and explicitly constructed the circuits to perform each of them. They are the following.



B.1 Computing the expected values of Hamiltonians with a certain grouping

In this section, we explain how to obtain the expected value of a Hamiltonian once we have grouped its Pauli strings. Let $H = \sum_{\alpha} h_{\alpha} P_{\alpha}$ be a multi-qubit Hamiltonian and suppose that the m first Pauli strings are compatible with a single HEEM measurement into the basis $\mathcal{B} = \mathcal{B}_1 \otimes \cdots \otimes \mathcal{B}_t$, with \mathcal{B}_i single or two qubit bases with $i = 1, \dots, t \leq m$. This means that the Pauli strings P_{α} with $\alpha = 1, \dots, m$ are diagonal in the basis \mathcal{B} . Let be $\vec{W}_P = \text{Diag}_{\mathcal{B}}\{P\}$ the vector with the diagonal entries of the Pauli string P in the basis \mathcal{B} . The elements of \vec{W}_P correspond to the eigenvalues of P , each of them repeated by its multiplicity. Thus, if \vec{P} is the probability distribution of a measurement on the basis \mathcal{B} , the expected value of the compatible Pauli strings is given by

$$\left\langle \sum_{\alpha=1}^m h_{\alpha} P_{\alpha} \right\rangle = \left(\sum_{\alpha=1}^m h_{\alpha} \vec{W}_{P_{\alpha}}, \vec{P} \right), \quad (5)$$

where (\cdot, \cdot) the inner product. In order to illustrate the procedure we are going to evaluate the energy of a very simple Hamiltonian consisting only of two Pauli strings,

$$H = 2IZY + 4ZXZ. \quad (6)$$

We have to check in Table 2 on which basis, if possible, these two strings can be measured together. After a careful look, we realize that the operators I and Z of the first qubits are compatible with Z , and that the operators XY and XZ of the second and third qubits are compatibles with $\tilde{\chi}$. The basis Z allows us to diagonalize the operators $I = +|0\rangle\langle 0| + |1\rangle\langle 1|$, and $Z = +|0\rangle\langle 0| - |1\rangle\langle 1|$, while the basis $\tilde{\chi}$ the 2-qubit operators

$$YX = -|\tilde{\chi}_0\rangle\langle\tilde{\chi}_0| + |\tilde{\chi}_1\rangle\langle\tilde{\chi}_1| + |\tilde{\chi}_2\rangle\langle\tilde{\chi}_2| - |\tilde{\chi}_3\rangle\langle\tilde{\chi}_3| \quad (7)$$

$$ZY = +|\tilde{\chi}_0\rangle\langle\tilde{\chi}_0| + |\tilde{\chi}_1\rangle\langle\tilde{\chi}_1| - |\tilde{\chi}_2\rangle\langle\tilde{\chi}_2| - |\tilde{\chi}_3\rangle\langle\tilde{\chi}_3| \quad (8)$$

$$XZ = +|\tilde{\chi}_0\rangle\langle\tilde{\chi}_0| - |\tilde{\chi}_1\rangle\langle\tilde{\chi}_1| + |\tilde{\chi}_2\rangle\langle\tilde{\chi}_2| - |\tilde{\chi}_3\rangle\langle\tilde{\chi}_3|. \quad (9)$$

One last important thing that we need is the explicit dependence of the vectors of the $\tilde{\chi}$ basis with respect to the computational basis, to correctly relate the vector of weights with the vector of outcomes

$$|\tilde{\chi}_0\rangle = +i|00\rangle - |01\rangle + i|10\rangle + |11\rangle \quad (10)$$

$$|\tilde{\chi}_1\rangle = +|00\rangle + i|01\rangle - |10\rangle + i|11\rangle \quad (11)$$

$$|\tilde{\chi}_2\rangle = +i|00\rangle + |01\rangle + i|10\rangle - |11\rangle \quad (12)$$

$$|\tilde{\chi}_3\rangle = -|00\rangle + i|01\rangle + |10\rangle + i|11\rangle. \quad (13)$$

See subsection B.2 for explicit expressions of how to construct every entangled measurement and the diagonal representation of pairs of observables in all of these bases.

Now we can tackle the problem of evaluating the energy of Eq. (6) with a measurement in the basis $\mathcal{B} = \mathcal{Z}_1 \otimes \tilde{\chi}_{2,3}$, where the subscripts refer to the subspace spanned by such qubits. For the Pauli string IZY we have $\text{Diag}_{\mathcal{Z}}\{I\} = [+1, +1]$ and $\text{Diag}_{\tilde{\chi}}\{ZY\} = [+1, +1, -1, -1]$. The vector \vec{W}_{IZY} is computed as the Kronecker product of the vectors $\text{Diag}_{\mathcal{Z}}$ and $\text{Diag}_{\tilde{\chi}}$. Thus,

$$h_{IZY}\vec{W}_{IZY} = 2 \times [+1, +1] \otimes [+1, +1, -1, -1] = [+2, +2, -2, -2, +2, +2, -2, -2]. \quad (14)$$

Analogously for the string ZXZ , we have $\text{Diag}_{\mathcal{Z}}\{Z\} = [+1, -1]$ and $\text{Diag}_{\tilde{\chi}}\{XZ\} = [+1, -1, +1, -1]$. Then

$$h_{ZXZ}\vec{W}_{ZXZ} = 4 \times [+1, -1] \otimes [+1, -1, +1, -1] = [+4, -4, +4, -4, -4, +4, -4, +4]. \quad (15)$$

Therefore, we have that

$$\sum_{\alpha=1}^m h_{\alpha}\vec{W}_{P_{\alpha}} = [+6, -2, +2, -6, -2, +6, -6, +2]. \quad (16)$$

In summary, what our algorithm does once it has identified which Pauli strings can be measured together is to check with which measurement basis it can do so and in which order those basis vectors have to be taken into account. After sorting out all the plus and minus signs, all is left to do is to multiply by the weight in the Hamiltonian h_{α} , and finally plug in the actual result of the experiment with Eq. (5).

	XX	YZ	ZY	YY	XZ	ZX	ZZ	XY	YX
XX	—	Ω^X	Ω^X	Bell	✗	✗	Bell	✗	✗
YZ	—	Ω^X	✗	✗	✗	✗	✗	✗	✗
ZY	—	✗	✗	$\tilde{\chi}$	✗	✗	✗	✗	$\tilde{\chi}$
YY	—	—	—	Ω^Y	Ω^Y	Bell	✗	✗	—
XZ	—	—	—	—	Ω^Y	✗	✗	—	$\tilde{\chi}$
ZX	—	—	—	—	—	✗	χ	✗	—
ZZ	—	—	—	—	—	—	Ω^Z	Ω^Z	—
XY	—	—	—	—	—	—	—	Ω^Z	—
YX	—	—	—	—	—	—	—	—	—

Table 2: Compatibility relation between two-qubits Pauli strings. The symbol \times indicates that the corresponding Pauli strings are not jointly measurable. The other boxes contain the entangled measurements that are compatible with the corresponding Pauli strings. See Appendix B.2 for the definitions of these measurements.

B.2 Jointly diagonalizable pairs in all entangled bases.

Bell :

$ \Phi_0\rangle = 00\rangle + 11\rangle$	Commuting pairs
$ \Phi_1\rangle = 00\rangle - 11\rangle$	$XX = + \Phi_0\rangle\langle\Phi_0 - \Phi_1\rangle\langle\Phi_1 + \Phi_2\rangle\langle\Phi_2 - \Phi_3\rangle\langle\Phi_3 $
$ \Phi_2\rangle = 01\rangle + 10\rangle$	$YY = - \Phi_0\rangle\langle\Phi_0 + \Phi_1\rangle\langle\Phi_1 + \Phi_2\rangle\langle\Phi_2 - \Phi_3\rangle\langle\Phi_3 $
$ \Phi_3\rangle = 01\rangle - 10\rangle$	$ZZ = + \Phi_0\rangle\langle\Phi_0 + \Phi_1\rangle\langle\Phi_1 - \Phi_2\rangle\langle\Phi_2 - \Phi_3\rangle\langle\Phi_3 $

Ω^X :

$ \Omega_0^X\rangle = + 00\rangle - i 01\rangle - i 10\rangle + 11\rangle$	Commuting pairs
$ \Omega_1^X\rangle = + 00\rangle - i 01\rangle + i 10\rangle - 11\rangle$	$YZ = - \Omega_0^X\rangle\langle\Omega_0^X + \Omega_1^X\rangle\langle\Omega_1^X - \Omega_2^X\rangle\langle\Omega_2^X + \Omega_3^X\rangle\langle\Omega_3^X $
$ \Omega_2^X\rangle = + 00\rangle + i 01\rangle - i 10\rangle - 11\rangle$	$XX = + \Omega_0^X\rangle\langle\Omega_0^X - \Omega_1^X\rangle\langle\Omega_1^X - \Omega_2^X\rangle\langle\Omega_2^X + \Omega_3^X\rangle\langle\Omega_3^X $
$ \Omega_3^X\rangle = - 00\rangle - i 01\rangle - i 10\rangle - 11\rangle$	$ZY = - \Omega_0^X\rangle\langle\Omega_0^X - \Omega_1^X\rangle\langle\Omega_1^X + \Omega_2^X\rangle\langle\Omega_2^X + \Omega_3^X\rangle\langle\Omega_3^X $

Ω^Y :

$ \Omega_0^Y\rangle = + 00\rangle + 01\rangle + 10\rangle - 11\rangle$	Commuting pairs
$ \Omega_1^Y\rangle = + 00\rangle + 01\rangle - 10\rangle + 11\rangle$	$XZ = + \Omega_0^Y\rangle\langle\Omega_0^Y - \Omega_1^Y\rangle\langle\Omega_1^Y + \Omega_2^Y\rangle\langle\Omega_2^Y - \Omega_3^Y\rangle\langle\Omega_3^Y $
$ \Omega_2^Y\rangle = + 00\rangle - 01\rangle + 10\rangle + 11\rangle$	$YY = + \Omega_0^Y\rangle\langle\Omega_0^Y - \Omega_1^Y\rangle\langle\Omega_1^Y - \Omega_2^Y\rangle\langle\Omega_2^Y + \Omega_3^Y\rangle\langle\Omega_3^Y $
$ \Omega_3^Y\rangle = - 00\rangle + 01\rangle + 10\rangle + 11\rangle$	$ZX = + \Omega_0^Y\rangle\langle\Omega_0^Y + \Omega_1^Y\rangle\langle\Omega_1^Y - \Omega_2^Y\rangle\langle\Omega_2^Y - \Omega_3^Y\rangle\langle\Omega_3^Y $

Ω^Z :

$ \Omega_0^Z\rangle = + 00\rangle - i 11\rangle$	Commuting pairs
$ \Omega_1^Z\rangle = + 00\rangle + i 11\rangle$	$XY = - \Omega_0^Z\rangle\langle\Omega_0^Z + \Omega_1^Z\rangle\langle\Omega_1^Z - \Omega_2^Z\rangle\langle\Omega_2^Z + \Omega_3^Z\rangle\langle\Omega_3^Z $
$ \Omega_2^Z\rangle = + 01\rangle + i 10\rangle$	$YX = - \Omega_0^Z\rangle\langle\Omega_0^Z + \Omega_1^Z\rangle\langle\Omega_1^Z + \Omega_2^Z\rangle\langle\Omega_2^Z - \Omega_3^Z\rangle\langle\Omega_3^Z $
$ \Omega_3^Z\rangle = + 00\rangle - i 10\rangle$	$ZZ = + \Omega_0^Z\rangle\langle\Omega_0^Z + \Omega_1^Z\rangle\langle\Omega_1^Z - \Omega_2^Z\rangle\langle\Omega_2^Z - \Omega_3^Z\rangle\langle\Omega_3^Z $

χ :

$ \chi_0\rangle = - 00\rangle + 01\rangle - i 10\rangle + i 11\rangle$	Commuting pairs
$ \chi_1\rangle = + 00\rangle + 01\rangle + i 10\rangle - i 11\rangle$	$XY = + \chi_0\rangle\langle\chi_0 - \chi_1\rangle\langle\chi_1 + \chi_2\rangle\langle\chi_2 - \chi_3\rangle\langle\chi_3 $
$ \chi_2\rangle = + 00\rangle - 01\rangle + i 10\rangle + i 11\rangle$	$YZ = - \chi_0\rangle\langle\chi_0 + \chi_1\rangle\langle\chi_1 + \chi_2\rangle\langle\chi_2 - \chi_3\rangle\langle\chi_3 $
$ \chi_3\rangle = - 00\rangle + 01\rangle + i 10\rangle + i 11\rangle$	$ZX = + \chi_0\rangle\langle\chi_0 + \chi_1\rangle\langle\chi_1 - \chi_2\rangle\langle\chi_2 - \chi_3\rangle\langle\chi_3 $

C Energy evaluation

In Table 3 we show the relative error for the energy evaluation of the GHZ state $|\psi\rangle = (|0\rangle^{\otimes N} + |1\rangle^{\otimes N})/\sqrt{2}$ for different molecule Hamiltonians and grouping methods. We fix the total number of shots to 2^{14} for all molecules, so the statistical error is large for big molecules. For molecules larger than H_2O , the best results are obtained with the HEEM grouping.

D Asymptotic scaling

In Fig. 4 a) we show the dependence of the number of groups on the total number of Pauli strings in the Hamiltonian of different molecules. We found that TPB obtains the largest number of groups for all molecules, while EM results in a significant reduction in the number of groups. HEEM obtains better results than TPB, but due to the constrain in the non-connected measurements, does not reach the results of EM.

However, in Fig. 4 b) we find a considerable improvement on the total number of CNOT gates. After the transpiling, taking into account a real quantum device architecture, EM needs more CNOT gates in order to

	TPB	EM	HEEM
<chem>H2</chem>	2.04%	0.31%	0.30%
<chem>LiH</chem>	3.13%	2.10%	2.04%
<chem>BeH2</chem>	10.65%	1.86%	3.17%
<chem>H2O</chem>	17.15%	12.70%	15.92%
<chem>CH4</chem>	38.56%	32.78%	14.17%
<chem>C2H2</chem>	52.8 %	46.4 %	43.7 %
<chem>CH3OH</chem>	47.3 %	79.1 %	43.9 %

Table 3: Relative error for the energy evaluation of the molecule Hamiltonians in the equilibrium distance for an initial GHZ state with different grouping methods. The simulation mimics the architecture, basis gate and noise of the quantum device *ibmq_montreal*. Each simulation has a total of 2^{14} shots evenly distributed across all measurements in each grouping.

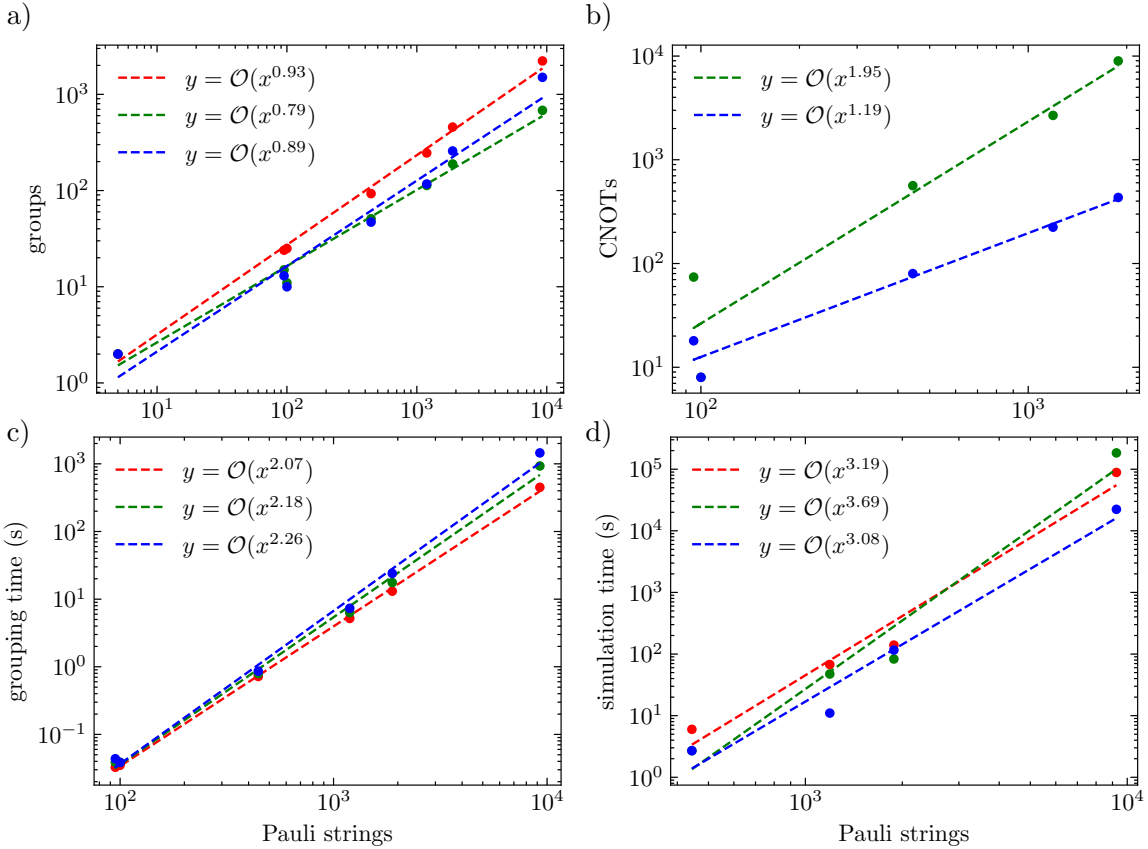


Figure 4: Dependence of a) the total number of groups, b) the number of CNOTs gates, c) CPU time for the grouping, and d) CPU time for the simulation of different molecules on the number of Pauli strings. The grouping algorithms used are TPB (red), EM (green), and HEEM (blue). The dashes colored lines represent a fit to the function $y = \beta x^\alpha$. Both in EM and HEEM uses the *ibmq_montreal* connectivity. In d) the simulation mimics the architecture, basis gate, and noise of the quantum device *ibmq_montreal*. Each simulation has a total of 2^{14} shots evenly distributed across all measurements in each grouping. The simulation is performed using the qasm HPC simulator provided by IBMQ. Transpiling and queue times are not included in these times.

perform SWAP gates between non-connected qubits. This problem is solved by using HEEM, which does not need any SWAP gate, resulting in less CNOT gates.

It is also important to consider the time needed to perform the grouping in a classical CPU, Fig. 4 c). All three algorithms start with the construction of the Pauli graph, which contains information about the commutative Pauli strings. Once the graph is obtained, TPB uses LDPC for the graph coloring which time complexity is $\mathcal{O}(n^2)$ where n is the total number of Pauli strings. EM makes use of a more sophisticated algorithm, which needs to run through the graph and check if it can group a pair of terms with any of the existing base. This extra check results in a slower algorithm. Furthermore, HEEM also checks if the grouping is compatible with the chip's connectivity.

However, despite the fact that the HEEM grouping is slower than the other methods, looking at the simulation

time, Fig. 4 d), it is clear that the reduction in the simulation time is notorious. Even if TPB circuits do not require CNOT gates, the number of circuits to simulate is much larger than that of HEEM. On the other hand, EM grouping results in lower circuits, but the number of SWAP gates needed to perform the simulation grows much faster than that of HEEM, making it the slower algorithm to simulate.